Published in final edited form as:
J Neural Eng. 2011 December ; 8(6): 066011. doi:10.1088/1741-2560/8/6/066011.

Mechanically adaptive intracortical implants improve the proximity of neuronal cell bodies

J P Harris[1,2], **J R Capadona**[1,2], **R H Miller**[3], **B C Healy**[4,5], **K Shanmuganathan**[6], **S J Rowan**[1,2,6], **C Weder**[6,7], and **D J Tyler**[1,2,*]

[1]Department of Biomedical Engineering, CWRU, 2071 Martin Luther King Jr. Drive, Wickenden Bldg, Cleveland, OH, 44106, USA [2]Rehabilitation Research and Development, L. Stokes Cleveland VA Medical Center, 10701 East Blvd. Mail Stop 151 AW/APT, Cleveland, OH 44106-1702 Cleveland, OH, 44106, USA [3]Department of Neurosciences, CWRU, 2109 Adelbert Road, Cleveland, OH, 44106, USA [4]Department of Neurology, Brigham and Women's Hospital, Partners MS Center, Harvard Medical School, 1 Brookline Place West, Suite 225, Boston, MA, USA, 02445, USA [5]Biostatistics Center, Massachusetts General Hospital, 50 Staniford St Suite 560, Boston, MA, USA, 02114, USA [6]Department of Macromolecular Science and Engineering, 2100 Adelbert Road, Kent Hale Smith Bldg, CWRU, Cleveland, OH, 44106, USA [7]Adolphe Merkle Institute and Fribourg Center for Nanomaterials, University of Fribourg, Rte de l'Ancienne Papeterie / P.O. Box 209, CH-1723 Marly 1, Switzerland

Abstract

The hypothesis is that mechanical mismatch between brain tissue and microelectrodes influences the inflammatory response. Our unique, mechanically-adaptive polymer nanocomposite enabled this study within the cerebral cortex of rats. The initial tensile storage modulus of 5 GPa decreases to 12 MPa within 15 minutes under physiological conditions. The response to the nanocomposite was compared to surface-matched, stiffer implants of traditional wires (411 GPa) coated with the identical polymer substrate and implanted on the contralateral side. Both implants were tethered. Fluorescent immunohistochemistry labeling examined neurons, intermediate filaments, macrophages, microglia, and proteoglycans. We demonstrate, for the first time, a system that decouples the mechanical and surface chemistry components of the neural response. The neuronal nuclei density within 100 μm of the device at four weeks post implantation was greater for the compliant nanocomposite compared to the stiff wire. At eight weeks post implantation, the neuronal nuclei density around the nanocomposite was maintained, but the density around the wire recovered to match the nanocomposite. The glial scar response to the compliant nanocomposite was less vigorous than to the stiffer wire. The results suggest that mechanically associated factors such as proteoglycans and intermediate filaments are important modulators of the response of the compliant nanocomposite.

Keywords

Brain; Neural Prosthesis; micromotion; cellulose; Cell encapsulation; electrode; Inflammation; Mechanical properties; Nanocomposite

[*]Correspondence and Reprint request should be directed to: Dustin J. Tyler (dustin.tyler@case.edu), Department of Biomedical Engineering, CWRU, 10900 Euclid Ave, Wickenden Bldg Rm 101, Cleveland, OH, 44106, USA.

The authors have no conflicts of interest related to this work to disclose.

1. Introduction

Despite the increasing evidence of the importance of cellular mechanotransduction on tissue repair and homeostasis (Clark *et al.*, 2007; Ingber, 2006), the role of mechanical mismatch has not been fully elucidated in an *in vivo* study to explain the interplay of chemical and mechanical factors that contribute to glial scarring surrounding intracortical implants. Previous research *in vitro* and *in silico* has supported the importance of mechanical signaling in several cell types in the brain. Cultured astrocytes have been shown to respond to mechanical stimuli via calcium signaling (Ostrow and Sachs, 2005). Investigations have shown that higher strain rates for cultured astrocytes lead to an increased reactivity (Cullen *et al.*, 2007). Cell types have responded differently to substrate stiffness as well. Notably, the rate of astrocyte and neuron proliferation as well as oligodendrocyte spreading and neuronal branching were influenced by substrate stiffness (Kippert *et al.*, 2009; Flanagan *et al.*, 2002; Georges *et al.*, 2006). Substrate stiffness is also known to shift cell differentiation in mesenchymal stem cells to be neurogenic, myogenic, or osteogenic (Engler *et al.*, 2006).

In addition to the effect of substrate stiffness, *in silico* modeling studies indicate that indwelling electrodes exert forces on local populations of cells (Lee *et al.*, 2005; Subbaroyan *et al.*, 2005; McConnell *et al.*, 2007). Over time, the implanted electrode is anchored to the tissue via the extracellular matrix and neural inflammatory cells (including microglia and astrocytes), resulting in cellular attachments to the electrode modifying the forces exerted on the brain tissue (McConnell *et al.*, 2007). Micromotion associated with electrode movement within the tissue and the mechanical properties of the electrode dynamically change the level of exerted forces on the cortical tissue during scar maturation. This phenomenon can also be exacerbated as a result of mechanically tethering the electrodes to the skull. *In vivo* studies which focus on the effects of electrode tethering have shown that untethered implants reduce the extent of the glial scar (Biran *et al.*, 2007; Kim *et al.*, 2004; Subbaroyan, 2007). It has been suggested that a reduced glial scar results from the reduction in forces applied to the tissue. Alternately, it has been proposed that less scarring is the result of limited meningeal ingrowth in response to untethered implants (Subbaroyan, 2007).

To investigate the effects of mechanical mismatch between the electrodes and the cortical tissue, several groups have developed electrode substrates and substrate coatings from materials such as polyimide, polydimethylsiloxane (PDMS), and parylene, which are more compliant than materials traditionally used to create electrodes. However, these materials have had limited success in attenuating glial scar formation. A limitation to many of these studies is that such materials still have moduli 6 orders of magnitude larger than that of the brain, while also introducing different surface chemistries that could confound the tissue-material interaction (Lee *et al.*, 2004; Nikles *et al.*, 2003; Takeuchi *et al.*, 2004; Wester *et al.*, 2009; Takeuchi *et al.*, 2005) and complicate the interpretation of these results. Of interest, surface treatments of electrode materials with a poly(vinyl alcohol)/poly(acrylic acid) hydrogel have reduced astrocyte reactivity, measured through the expression of glial fibrillary acidic protein (GFAP) (Lu *et al.*, 2009).

Given the evidence for the contribution of mechanical force to the glial scar from *in vitro*, *in silico*, and *in vivo* experiments, we hypothesize that the *in vivo* glial scar response is influenced by a chronic stiffness mismatch between the soft brain tissue and stiff intracortical implants. To create an *in vivo* device to characterize the importance of mechanical compliance of intracortical implants on both the chronic inflammatory reaction and the long-term electrode performance, we used our recently developed mechanically adaptive polymer nanocomposite, previously described in detail (Capadona *et al.*, 2007; Capadona *et al.*, 2008; Capadona *et al.*, 2009; Shanmuganathan *et al.*, 2010a, b, 2009). Our previous work has demonstrated that the polymer nanocomposite can reduce its tensile

storage modulus from 5 GPa to 12 MPa within 15 minutes upon exposure to simulated physiological conditions in artificial cerebral spinal fluid (ACSF) at 37°C (Capadona *et al.*, 2007; Capadona *et al.*, 2008; Capadona *et al.*, 2009; Shanmuganathan *et al.*, 2010a, b, 2009). The polymer nanocomposite has modest aqueous swelling of 60–75%, in comparison to the several hundred percent exhibited by hydrogel approaches. Here, we have created model electrodes from the adaptive polymer nanocomposite (NC) material. We have demonstrated that the nanocomposite material performs similar *in vitro* and *in vivo* (Harris *et al.*, 2011). While the previous work performed modest histological analysis, this is a more complete histological report on their use as cortical implants demonstrating that there are both foreign body elements, as well as mechanical effects, contributing to the overall tissue response at the biotic-abiotic interface. These components of the inflammatory response appear to be separate, but intricately coupled to the neuronal response.

2. Materials and Methods

2.1. Implant Fabrication and Imaging

Implants consisted of two types, referred to as nanocomposite (NC) and wire. NC implants were created by casting films from a dimethylformamide (DMF) solution of poly(vinyl acetate) and tunicate whiskers as reported previously (Capadona *et al.*, 2008). The NC had a cellulose whisker content of 15% w/w. The resulting films were used to create sheets via a custom mold in a hot press (Carver, Wabash, IN). Sheets were used to create 3 mm long probes that measured 100 ± 5 μm in thickness and 203 ± 19 μm in width with an approximately 45 ± 3° angle tip (figure 1a) via a cutting process. The cutting process created a nanocomposite with two types of surfaces: two pressed sides (figure 1c) and two cut sides (figure 1d). Both implant types were single shank probes with nearly the same cross-sectional area Refer to (Harris *et al.*, 2011) for a characterization of implant mechanical properties the NC material.

Wire implants consisted of 50 μm diameter tungsten wires (AM-Systems, Sequim, WA) from which the Teflon insulation was mechanically stripped using cutting tweezers. Wire implants (figure 1b) were dip-coated in a solution of poly (vinyl acetate) (PVAc, MW 113,000g/mol, density 1.19g/cm^3, Sigma Aldrich) in toluene at a concentration of 10% w/w at 70°C. A droplet of PVAc was placed on the edge of a glass dish and the tungsten wire was steadily dragged through the drop repeatedly about twenty times or until the coated wire had a diameter of ~ 160 μm. Samples were then cut into 3mm long sections, and with the aid of a microscope, sections of uniform diameter of 160 μm were selected for implantation.

A scanning electron microscope (SEM) imaged the NC and wire implants at high magnification. Both the NC and wire implants were covered with a thin layer of Palladium, approximately 7–10 nm. The samples were then attached to a chuck with Teflon tape and placed inside the S-4500 Hitachi SEM. Samples were imaged at various magnifications and angles (figure 1c–e).

2.2. Water Contact Angle

To analyze the surface hydrophilicity of the two implants, water contact angle measurements were performed on sheets of the nanocomposite and neat PVAc. Sheets of nanocomposite were made as described above, and the fabrication of neat polymer sheets was performed as described in previous literature (Harris *et al.*, 2011). The FTA 200 (First Ten Angstroms, Portsmouth, VA) instrument dispensed and imaged droplets on the sheets. Three to five samples from sheets were imaged, and the FTA32 software program analyzed the water contact angle. On the image, the user set the base of the droplet and one fourth of the

envelope of the drop. The program calculated the angle using the base and envelope of water droplet.

2.3. Surgical Procedures

All surgeries were performed under sterile conditions with autoclaved instruments. Both wire and NC implants were sterilized via an autoclave before implantation. The modulus of NC implants was measured and verified to be unaltered by the autoclave process (data not shown). The same surgeon performed all surgeries while an assistant monitored anesthesia levels and manipulated equipment. All procedures were approved by the Case Western Reserve University Institutional Animal Care and Use Committee (CWRU IACUC) and minimized pain and discomfort of the animal.

Male Sprague-Dawley rats from 206–335g were implanted bilaterally with a wire and a NC probe. The implants were affixed to sterile ceramic forceps tips (Fine Science Tools, Foster City, CA) with glucose. Anesthesia was induced via an intraperitoneal injection of ketamine (80 mg/kg) and xylazine (10 mg/kg). After the animal reached the surgical plane, as determined by lack of response to toe pinch, the animal's head was shaved and eyes protected via sterile ocular lubricant. A circulating water mat was placed underneath the animal while the animal was fitted with a thermometer and pulse oximeter (Surgivet, Waukesha, WI) to monitor vitals. The animal was secured on a stereotaxic frame (Stoelting Co., Wood Dale, IL) fitted with a gas mask. The animal was ventilated (Engler, Hialeah, FL) with oxygen; once the animal started to come out of the initial ketamine/xylazine induction (determined by whisking, reacting to toe pinch, raised heart beat), Isoflurane (1–3%) was introduced to oxygen flow to maintain a surgical level of anesthesia.

After securing the animal, marcaine (~0.1 mL, diluted 1:5 with saline) was injected before incision as a local anesthetic, and the head area was sterilized with betadine and alcohol. An incision along the midline exposed the skull. Skin was retracted using an eye speculum. Bilaterally, a 3 mm biopsy punch (Miltex, York, PA) was used to drill 2 implant sites centered 4.5 mm caudal to the bregma, 3 mm lateral to the midline. The biopsy punch prevented heat damage caused by motorized drills and provided a well-defined 3 mm opening. Three screws were implanted for later fixation of dental cement. For both openings, one screw was placed 1 mm caudal to the biopsy punch-produced openings. The remaining screw was placed 4mm rostral to the biopsy hole on the animal's left side. After three 0–80 × 3/32 screws were attached to the skull, a fine 45° angle microprobe (Fine Science Tools, Foster City, CA) was used to create an opening in the dura (approximately 1 mm diameter) for both implant sites. After manually lowering the implant to the surface of the brain, an automated mechanical inserter controlled by LabView 7.1 (National Instruments, Austin, TX) inserted the implants 2 mm into the tissue at a rate of 2 mm/s. A 1 mm tab was left exposed above the brain tissue to enable tethering via Kwik-Sil (WPI Inc, Sarasota, FL). Kwik-Sil sealed the implant sites, and dental cement (Stoelting, Wood Dale, IL) was applied to cover the implant sites and screws. The skin was sutured with 5-0 polypro sutures (Henry Schein, 1016409, Melville, NY) enclosing the dental cement headcap. Each animal received one wire and one NC implant in random order and side placement.

After surgery, an animal was isolated in a clean cage on a warm water blanket and monitored every thirty minutes until sternal. One antibiotic shot of cefazolin (20 mg/kg) and one analgesic shot of buprenorphine (0.01 mg/kg) were given on the day of surgery. Two cefazolin shots, same dose, were given the day following surgery, while buprenorphine was given as needed. No steroids were applied at any time throughout the implant period. Each rat was monitored regularly after surgery for signs of distress, weight loss, and dehydration. In rare cases, complications with infections and sutures caused early euthanasia and these animals were removed from the study. In the remaining animals, some animals exhibited a

large void around the implant. The response was analyzed and determined to be a result of excessive bleeding after implantation. These hemispheres were excluded from analysis since the response was due to insertion trauma rather than the response to the implant.

2.4. Fixation, Tissue Preparation, and Immunohistochemistry

After the designated timeframe, four or eight weeks, animals were euthanized by transcardial perfusion. Animals were first anesthetized to a surgical plane as described above. Perfusion rate was controlled via a mechanical pump (VWR, West Chester, PA) with 500 mL of D-PBS (Invitrogen, Carlsbad, CA) or when no trace of blood was seen exiting the right atrium. Approximately 250 mL of 10% buffered formalin (Fisher, Pittsburgh, PA) fixed the tissue of the animal. The brain and probes were placed in formalin for 24 hours, after which the brain was then transferred to fresh formalin. The brain remained in fresh formalin for up to one week, until it was cryoprotected in 30% sucrose solution.

After removing the probes, brains were frozen in embedding molds (Electron Microscopy Products, Hatfield, PA) containing OCT compound (Sakura, Tokyo, Japan) and mounted and sectioned horizontally by a cryostat (Thermo Fisher Scientific, Waltham, MA) creating 30 μm thick slices. Slices chosen were spread over the whole length of the implant while remaining slices were preserved in cryoprotectant solution (Watson *et al.*, 1986). Following procedures outlined previously (Biran *et al.*, 2005), slices were labeled via a free-floating protocol.

Briefly, slices were placed in blocking solution overnight at 4°C. Blocking solution was composed of 4% (v/v) normal goat serum (Sigma-Aldrich, St. Louis, MO), 0.3% (v/v) Triton-X-100 (Sigma-Aldrich), and 0.1% (w/v) sodium azide (Sigma-Aldrich) in 1× D-PBS (Invitrogen, Carlsbad, CA). Slices were then placed in fresh blocking solution with primary antibodies (table 1) overnight at 4°C. On the third day slices were placed in blocking solution with secondary antibodies, goat anti-rabbit IgG or anti-mouse IgG1 or IgM, Alexa Fluor 594, 488, and DAPI dilactate (Invitrogen, Carlsbad, CA) for one hour at room temperature. After primary and secondary application periods, three, 15 minute washes in PBS were performed on a shaker. Slices were mounted and cover slipped using Fluoromount-G (Southern Biotech, Birmingham, AL).

2.5. Image Acquisition and Analysis

Images of slices were taken by an Axio Imager.Z1M Microscope and AxioCam MRm CCD camera (Zeiss, Thornwood, NY). Implant sites were centered in the field, and exposure settings were set to prevent overexposure. The settings were then maintained the same for the whole set of stained images. Four automated exposures were performed on every site: one bright field and 3 fluorescent colours. Seventeen animals with bilateral implants were analyzed at four weeks. After removing hemispheres with excessive insertion trauma, there were 11 trials for the wire and 16 for the NC. Seven animals were analyzed after eight weeks. Statistical analysis based on prior work predicted that about 10 animals were needed for analysis. On average, three slices were used per animal for a given label.

A custom Matlab R2009b (MathWorks, Natick, MA) script was developed to measure the intensity around the implant. The script automatically detected the border and area of the implant based on the bright field image. Bright field images were used for border detection since it was difficult to see the actual border in fluorescent images. Therefore, some fluorescent images appeared to have a larger implant area than actual. This effect and the variable shrinkage of tissue during histology contribute to the apparent variation in size of implants pictured in fluorescent images. Calculating the size of the implants in images, the

average sizes of the implants were similar. 23,329 ± 3279 μm^2 for NC and 24,513 ± 5264 μm^2 for wire.

One hundred, equally spaced, radial lines emanated from the centroid of the implant area. For each one of the 100 rays, the intensity (pixel values) over the first 200 microns immediately external to the border were measured around the implant site (figure 2a). The average intensity of the 100 rays was divided by the background measurement of the image to account for differences between images due to photobleaching and other effects inherent in fluorescent immunohistochemistry. Background intensity values were measured per image at the edge of the image, at least 300 μm from the implant and outside the region measured for the response. Several measurements were made for each image including peak intensity, near integral intensity (0–50 μm), and far integral intensity (50–100 μm) as well as certain intervals dictated by the data and highlighted in the text.

For certain IHC labels, an additional evaluation of IHC intensity was performed to determine the effect of the nanocomposite side on the response. A subset of the 100 rays were averaged to measure intensity of the pressed sides versus the cut sides of the nanocomposite. Based on the cutting technique used to create the probes, the pressed side was the longer of the two sides. The majority of images analyzed had clearly discernable long and short sides. Images with indistinguishable sides were left out of analysis. Approximately 10 of the 100 rays were used to determine image intensity based on a single side. For each slice, the two long sides were averaged together and the two short sides were averaged together. Therefore, approximately 20 of the 100 rays determined the reaction to the cut sides, and a separate 20 of the rays determined the reaction for the pressed sides. The first 20 μm and 50 μm of the intensity were examined for DAPI and ED1 to examine the effect of the surface roughness on the tissue response. A mean intensity was computed over the distance as well as the 95% confidence interval of the mean intensity. DAPI analysis was performed to analyze the total cell density around the implants. Analysis of ED1 was performed since previous literature has indicated that ED1 positive cells are often closest to the implant (Biran *et al.*, 2005).

The automatic detection removed human error across samples, but could result in the inclusion of up to 3–5 μm of the image without tissue, which could slightly distort data in this range. The distance between the implant and the peak tissue response error is within 5 μm, but is consistent between the experimental conditions and does not affect the results of this work.

Another custom Matlab script used the same border detection algorithm, but computationally isolated and highlighted nuclei (figure 2b). After the automated marking, an investigator manually reviewed the identification and added or subtracted nuclei missed by the algorithm. After marking, Matlab computed the distance from each nucleus to the border along the ray emanating from the centroid of the implant site. These distances were binned into 10 μm increments, and a histogram was created for the number of nuclei. The counts were scaled by dividing by the area of the corresponding 10 μm-wide concentric polygonal donut to provide the neuron density.

2.6. Statistics

In order to estimate the effect of the implant type on the outcome, the differences between measured values (e.g. the peak intensity, integrals, cell count, etc.) were modeled using a multilevel model. The model (Equation 1) included a baseline level for the outcome (β_0), a fixed effect for the difference in the outcome based on the implant type (β_1), a random effect for each animal ($b_{0,i}$), a random effect for each slice within each animal ($c_{0,ij}$), and residual error (e_{ijk}):

$$Outcome_{ijk}=\beta_0+\beta_1{}^{*}IMPLANT\_TYPE_{ijk}+b_{0,i}+c_{0,ij}+e_{ijk} \quad (1)$$

where i indexes the rat, j indexes the slice, and k indexes the side. If β_1 was significantly different than zero, the implant had a significant effect on the outcome of interest. All statistical analysis was completed in the statistical package R (R Foundation for Statistical Computing, Vienna, Austria) (R Development Core Team, 2009; Pinheiro *et al.*, 2009).

3. Results

3.1. Water Contact Angle

Water contact angle measures show that there is no significant difference between the hydrophobicity of the PVAc wire coating and the PVAc-NC material being studied. The nanocomposite had a contact angle of 70.3 ± 2.2° and the neat material had a contact angle of 64.0 ± 3.1°. A two sample t-test did not show any significant differences in the contact angle (p=0.22).

3.2. Neuronal Nuclei

NeuN (neuronal nuclei) labeled cells showed neuronal nuclei around the probe (figure 3). There is a reduction of neuronal density towards the tissue-implant border for both implants. At four weeks, however, the neuronal density within 200 μm of the nanocomposite (NC) implant is significantly greater than it is around the wire (figure 3a,b). At eight weeks, the neuronal density around both implants types is no longer significantly different at any distance from the implant (figure 3a,b). For the wire, the neuronal density within a radius of 20 μm from the interface is significantly greater at eight weeks than four weeks (p=0.04). The data at other intervals is not statistically significant, but trends indicate that neuronal density around rigid wire implants increases between four and eight weeks to a density similar to the NC at both four and eight weeks. Further, there are no trends in decreasing neuronal nuclei density between four and eight weeks with the NC.

Representative images of NeuN for c) four week NC, d) four week wire, e) eight week NC, and f) eight week wire. Scale bars 100 μm.

3.3. Astrocytes

Analysis of GFAP labeling indicates the reactive astrocytic response. The intensity of GFAP labeling peaks approximately 10–20 μm from the tissue-implant border and gradually decreases further away (figure 4a,b). For both four and eight week data, the 0–50 μm region from the implant exhibits hypertrophied astrocytes with a reactive morphology (figure 4c–f, 4c inset). Astrocytes outside of 200 μm do not exhibit GFAP labeling (figure 4c–f). At four weeks, the maximum intensity and 0–50 μm integral of intensity are not significantly different between tissue around wire and NC implants, though the 50–100 μm intensity integral is significantly greater (p=0.05) for wire samples compared to NC at four weeks. At eight weeks, the intensity maximum is significantly greater around the wire implants than the NC implants (p=0.04), and the intensity integral from 25–100 μm around wire implants is significantly less than the NC (p=0.03). There are no statistical differences for GFAP intensity with wire samples between four and eight weeks, but the labeling for GFAP around the nanocomposite at eight weeks is significantly greater over the 20–80 μm interval than at the four week timepoint (p=0.03). Additionally, GFAP labeling tends to be more diffuse or less compact around the NC than the wire at eight weeks (figure 4b, e, f).

3.4. Proteoglycan

Chondroitin Sulfate Proteoglycan (CSPG) is a structural component of extracellular matrix and its upregulation within the glial scar has been linked to inhibition of axonal outgrowth (Silver and Miller, 2004). Intensity for CSPGs, via labeling for CS56 antibodies (table 1), peaks within 15 μm from the border (figure 5a–f). The peak around the NC implant returns to baseline by 50 μm for the four and eight week samples implanted with NC; levels remain elevated around the four week wire implant up to 150 μm. The wire implants at eight weeks feature a response that returns to baseline by 100 μm from the tissue-implant border (figure 5b,e,f). CS56 labeling at four weeks was significantly greater around the wire than NC starting at 10 μm and extending out to 150 μm ($p<0.01$) (figure 5a,c,d). At eight weeks, the peaks and integrals were similar for tissue around NC and wire implants.

3.5. Vimentin

Vimentin labeling is associated with immature astrocytes, extracellular matrix components, and developing axons (Alonso, 2005; Pekny, 2003; Levin *et al.*, 2009). At both timepoints, vimentin expression is upregulated with a peak at 10 μm from the implant (figure 6a–f) and decreases to baseline levels by 100–150 μm from the implant border. At four weeks (figure 6a,c,d), the vimentin intensity maximum and 0–32 μm intensity integral for NC implants is significantly greater than for the wire implants ($p<0.01$). Note that at 32 μm there is an intersection of the two implant profiles. At eight weeks (figure 6b,e,f), measures of vimentin labeling are not significantly different between the NC and wire. In the interval of 10–150 μm from the tissue-implant border, the intensity integral around the wire significantly decreased from four to eight weeks ($p=0.03$).

3.6. Macrophages/Microglia

Analysis of IBA1 and ED1 labeling quantified the density of activated microglia and macrophages. IBA1 labels all microglia (figure 7a–f) and ED1 labels (figure 8a–f) activated microglia and activated macrophages. Microglia as shown by IBA1 labeling appeared punctate or amoeboid near the border and a ramified morphology away from the implant site. The microglia response was characterized by intense IBA1 labeling 10 μm from the border that rapidly decreased to near background levels at more than 100 μm from the border. ED1 labeling (figure 8a–f) exhibited similar features but was limited mainly to amoeboid cells close to the implant interface.

The four and eight week IBA1 maximum intensity (figure 7a–f) from tissue around the NC is significantly greater than the intensity from tissue with wire implants at the same time point ($p=0.02$, $p<0.01$). The 0–150 μm intensity integral is significantly greater from samples around the eight week NC than from the eight week wire (figure 7b,e,f). Response changes for a particular implant type are not significant between four and eight weeks.

The peak intensities of ED1 at four and eight weeks are not significantly different between the NC and the wire (figure 8a–f), but the 17–150 μm intensity integral is significantly greater for wire implants compared to NC at four weeks ($p=0.03$). The 0–150 μm ED1 intensity integral significantly decreases for the wire from four to eight weeks ($p=0.04$). The 0–50 μm ED1 intensity integral is significantly greater for the nanocomposite compared to wire implants at eight weeks ($p=0.03$) (figure 8b,e,f).

3.7. IHC intensity based on NC side

To examine the effect of surface roughness on the IHC response, we examined DAPI and ED1 labeling across many animals. Several different examinations of intensity were examined, but no examination yielded significant effects based on side. The complete numbers are shown in Table 2. Similar intensity between sides indicates that the difference

of mean intensities between sides is less than the 95% confidence interval. A sign test for the paired data was performed to determine if the there was a statistically significant difference based on side. The results indicate that side does not have a significant effect on the tissue response.

4. Discussion

The results presented here support the hypothesis that the mechanical mismatch between brain tissue and microelectrodes influences the inflammatory response. Specifically, we found that the implant stiffness affects the neuronal response and composition of the glial scar, as the NC implanted animals had a significantly greater neuronal density than the wire implants at four weeks. These results aligned with previous studies that reported neuronal nuclei density was reduced around the implant in conjunction with similar upregulation of identical glial scar factors (Winslow and Tresco, 2009; Biran *et al.*, 2005; Zhong and Bellamkonda, 2007).

In this work, we implanted nanocomposite probes and neat PVAc coated tungsten wires. To confirm that surface roughness and morphology were not factors in the response, we analyzed the nanocomposite and neat PVAc. Examination via SEM showed that the neat polymer had a smooth surface (figure 1e), and the nanocomposite had two sides of different roughness. The pressed side of the nanocomposite had a smooth surface with only minor indentations (figure 1c). The cut side of the nanocomposite had a rough surface (figure 1d). Under 50,000× magnification (figure 1d, inset), the tunicate whiskers of the nanocomposite were clearly evident and protruded on the cut edge.

Next, we examined whether differences in surface roughness were contributing to the tissue response. There are two distinct sides with different surface roughness, and we investigated whether the side affected the tissue response. The examination of the response based on side indicated that the response was similar between the two sides of the nanocomposite. These results support that surface roughness did not affect the tissue response. From SEM images, the surface roughness differences between wire and nanocomposite were much less than the differences between sides of the nanocomposite. Collectively, the data suggests that our observed differences in tissue response are not due to differences in surface roughness. Our findings agree with previous research that has shown that the surface roughness of implant does not effect the tissue response past 4 weeks (Szarowski *et al.*, 2003).

To further examine the nanocomposite and the neat polymer, we investigated the surface chemistry via water contact angle. The nanocomposite and neat polymer had similar water contact angles. Since the two materials had a similar hydrophobicity, the data suggests that surface chemistry was not drastically modified by the insertion of tunicate whiskers into the neat polymer. Therefore, the analysis of the nanocomposite and neat polymer suggests that any effect of surface roughness and surface chemistry should be contributing similarly, if at all, to the different tissue responses to the materials.

The tissue response in our results was similar to previous reports (Winslow *et al.*, 2010; Winslow and Tresco, 2009). However, in our case, the classical markers of the glial scar (GFAP and ED1) do not fully explain the differences seen in neuronal density around each of the implant types at four weeks. Though the softer nanocomposite implant had a significantly greater neuronal density around the probe than the rigid wire after four weeks, there was not a significant difference in GFAP or ED1 labeling (peak or 0–50 μm interval). In the 0–50 μm interval nearest to the device, considered critical for unit recording, the brain tissue around the NC implants had nearly twice the neuronal density than that around the

wire implants at four weeks that may improve recording of single units from neurons located close to the implant at that time period (Buzsáki, 2004).

Examining the correspondence of GFAP and neural density in our results, GFAP did not account for all the differences seen between neuronal densities around the implant types. Specifically at four weeks, the GFAP peak intensity and the 0–22 μm intensity integrals were similar for both implant types while there was a significant difference over the same range for neuronal density. This may be due to the wide assortment of roles, both positive and negative associated with astrocytes. Astrocytes have been implicated in several different functions associated with cytoskeletal structure including neurotransmitter maintenance and blood brain barrier function (Simard *et al.*, 2003; Ortinski *et al.*, 2010). GFAP positive cell functions can be neuroprotective, as transgenic animals without GFAP show a larger functional deficit after injury (Faulkner *et al.*, 2004). Detrimental to neural protection, astrocytes have been implicated as a diffusion barrier (Roitbak and Sykova, 1999), remyelination limiter (Fawcett and Asher, 1999), and producer of cytokines and extracellular matrix components such as fibronectin (Shearer *et al.*, 2003) and CSPGs (McKeon *et al.*, 1999). Since astrocytes have been tied to many structural components including cytoskeletal arrangement and secretion of ECM components, it is believed that GFAP would be a key component in mechanical signaling. Therefore, it is notable that the rigid wire created a wider radius of GFAP activation at four weeks, but a more compact scar at eight weeks. A wider radius is suggested by a nearly significant difference over 22–150 μm intensity interval ($p=0.06$) and a significant difference over the 50–100 μm intensity integral ($p=0.05$) at four weeks (figure 4a,c,d). Further, the peak intensity of GFAP expression was larger for the wire ($p=0.04$), yet the distribution of GFAP expression was broader for the NC at eight weeks (25–100 μm, $p = 0.03$, figure 4b,e,f). From four to eight weeks, the neuronal response (NeuN) and GFAP labeling around the NC implant was unchanged. This suggests the NC formed a static scar. Yet, with wire implants, the GFAP expression at eight weeks became more compact, and NeuN positive cells in the same region of tissue appeared to increase around wire implants. The results from wire implants suggest that the scar is continuing to compact and remodel in response to the greater mechanical stiffness.

Cytoskeletal components play a major role in the ability of a cell to interface with and respond to the extracellular environment. The type and quantity of the filament are important in determining the ability of the cell to respond to the mechanical environment and move through the extracellular space (Alberts, 1994). In addition to GFAP, vimentin is an intermediate filament expressed in astrocytes and was investigated here (see (Pekny, 2003) for a review). In contrast to GFAP, the peak intensity and 0–32 μm intensity integral for vimentin labeling were significantly greater at four weeks for the NC, compared to the wire. Historically, vimentin has been tied to immature astrocytes, but recent research has linked vimentin expression to rapid neurite extension in response to damage (Levin *et al.*, 2009). Likewise, NG2+ cells that express vimentin have been proposed to support repair of central nervous system (CNS) damage, and stabilize axons in response to dieback from ED1+ cells (Alonso, 2005; Nishiyama, 2007; Busch *et al.*, 2010). Here, the increase in vimentin labeling around four week implants was associated with more neurons around NC implants than wire implants (figure 6a,c,d, 3a,c,d). This is consistent with potential neuroprotective implications for vimentin positive cells. Thus, we believe the correlation is due to positive effects associated with the intermediate filament vimentin. At eight weeks, the contrast in vimentin levels was no longer evident, which also correlates with similarity in neuronal densities around each implant type, further supporting the role of the intermediate filament, vimentin in supporting the neuronal density around the cortical implant. We believe that these results suggest that the expression of intermediate filaments in the tissue surrounding our implants is related to the mechanical properties of the electrode material.

To further examine the role of mechanics in the wound healing response, we examined another component of the glial scar, proteoglycans. Proteoglycans are negatively charged polysaccharide chains, and are an important structural constituent of the extracellular matrix (ECM) (Alberts, 1994). When found in elevated concentrations within tissue, the high density of negative charges found across their backbone have been shown to sequester cations, causing large amounts of water to diffuse out of adjacent tissue, into the proteoglycan rich areas. This phenomenon creates a swelling pressure that enables the tissue to withstand compressive forces. A subclass of proteoglycans secreted by astrocytes, Chondroitin Sulfate Proteoglycan (CSPG), has been shown to be deposited by astrocytes in gradients of increasing concentration towards the injury site (Silver and Miller, 2004). Interestingly, our results indicated that the area with elevated CS56 labeling (label for CSPGs,) is much larger around the wire implants than around the NC at four weeks (figure 5a,c,d). This is in agreement with previous research demonstrating that CSPGs inhibit neuronal outgrowth (Silver and Miller, 2004; Busch and Silver, 2007; Fawcett and Asher, 1999), further supported by our four week NeuN staining (figure 3a,b,c,d). Additionally, *in vitro* experiments have shown increased CSPG labeling in response to increased strain (Cullen *et al.*, 2007), further supporting our hypothesis that the mechanical mismatch between brain tissue and microelectrodes influences the response.

While our results provide interesting insights into the NC, reduced mechanical forces, and improved neuronal densities, we cannot ignore the cofounding effects of the inflammatory mediating microglia cells. Microglia and macrophage cells mediate the inflammatory and immune response to minimize bacterial/viral invaders (Kreutzberg, 1996). Macrophages have also been implicated in axonal dieback (Horn *et al.*, 2008). Many studies of the tissue response to intracortical electrodes have focused on macrophage activation in response to indwelling implants (Biran *et al.*, 2005). Activated macrophages and microglia, as labeled by ED1, were similar for peak intensity and the 0–17 μm (border to divergence point) intensity integral at four weeks (figure 8a,c,d). Similar to the GFAP and CSPG responses, there is a greater radius of ED1 activation in tissue around the wire implants at four weeks; the 17–150 μm intensity integral was greater for wire implants at four weeks. At four weeks, increased ED1 activation can be loosely associated with decreased NeuN labeling over similar distance from the electrode tissue interface. At eight weeks, ED1 activity was less pronounced around wire implants (figure 8b,e,f), which corresponded to an apparent recovery in NeuN positive tissue.

While ED1 labels only activated macrophages and microglia, IBA1 marks all microglia and macrophages. The four and eight week IBA1 maximum intensity (figure 7a–f) from tissue around the NC was significantly greater than the intensity from tissue with wire implants at the same time point ($p=0.02$, $p<0.01$). Differences between IBA1 and ED1 labeling can therefore be attributed to the presence of either resting microglia or a subset of beneficial, “alternatively activated” (M2), macrophages (Kigerl *et al.*, 2009). The ED1 peak intensity was similar between the two implant types at four weeks, but the IBA1 peak for NC was 18% greater than the wire, indicating the presence of microglia cells independent of levels of activated cells (ED1) (figure 7a,c,d, 8a,c,d). For the NC implants, the presence of additional non-ED1 reactive microglia and higher neuronal density at four weeks may indicate a beneficial role of microglia. Regardless of the state of the macrophages/microglia, the results suggest an ongoing reaction for both implant types since activated macrophages should return to baseline 21 days after a stab injury to cortex (Fujita *et al.*, 1998; Nisbet *et al.*, 2009). Our results are consistent with research showing a sustained response to indwelling implants (Winslow *et al.*, 2010; McConnell *et al.*, 2009).

Indicators of the glial scar components suggest that mechanics continues to modify the glial scar at eight weeks. Although, the mechanical-associated labels, GFAP and CS56, no longer

show a similar increased radius of activation around wire implants at eight weeks, GFAP labeling (figure 4b,e,f) around wire implants exhibit a more compact, higher peak than the compliant NC implants. Prior work (Frampton *et al.*, 2010) hypothesizes that a more compact GFAP response increases the impedance of an electrode which may decrease the quality of electrode recordings. Aligning with previous research (Fujita *et al.*, 1998; Nisbet *et al.*, 2009), both implant types appear to lowered ED1 activation from four to eight weeks (figure 8a–f) suggesting an ongoing reaction that lessens over time. The 0–50 μm intensity integral for ED1 and IBA1 was significantly greater around NC implants than the wire implants at eight weeks (figure 7b,e,f and 8b,e,f), but further work is needed to determine whether the difference is neuroprotective, neurotoxic, or neither at longer time points. Regardless of the similar neural densities at eight weeks, the nanocomposite continues to modify the overall tissue response up to eight weeks.

Another possible interpretation of the data is that softer implants are affecting the time-course of the response rather that final results, and hence, similar neuronal densities at eight weeks. It is known that the insertion event causes trauma, but it is unknown how stiffness might affect the repair of this trauma. Previous research has shown the response past four weeks is independent of size, shape, and surface roughness (Szarowski *et al.*, 2003), but the softer nanocomposite may allow for quicker repair of insertion damage. The increased levels of vimentin and IBA1 at four weeks could indicate a more robust healing process. Additionally, the similar neuronal densities between NC and wire at eight weeks coupled with the recovery of the neuronal density around wire implants to nanocomposite levels could suggest a quicker repair around NC implants. In this paper, our goal was to demonstrate that there is an effect based on probe stiffness. Further experiments are necessary to clearly describe the time course of the response and the specific effects of probe mechanics on that time course.

In summary, the four and eight week results show that the nanocomposite material modifies the glial scar and neuronal density around implants in comparison to stiffer wire implants. Four week nanocomposite implants feature greater neuronal densities than wire implants, and several glial scar labels such as GFAP, CSPG, and ED1 show a larger radius of activation from the implant-tissue border around wire implants than NC implants. Notably GFAP and CSPGs, structural components, suggest the involvement of mechanics in the tissue response. Eight week results provide further evidence that the response to implants is ongoing, dynamic, and modified by the nanocomposite. Results show that the nanocomposite can maintain its neuronal density for at least eight weeks despite macrophage/microglia activation.

5. Conclusions

By utilizing our mechanically adaptive polymer NC materials, it is possible to separate the foreign body response to the implanted electrodes from the effect of material stiffness. While mechanical properties of the materials correlate to differences between neuronal densities at four weeks, we also demonstrate that the NC parallels the response to the field-leading wire at eight weeks (Winslow and Tresco, 2009; Winslow *et al.*, 2010). Our data also suggest the importance of controlling vimentin and CSPG response to improve neuronal density. Through the use of the mechanically adaptive nanocomposite, we demonstrate a system that can decouple the mechanical and surface chemistry components of the neural response. We expect this to be a valuable tool in future research regarding cortical tissue. Our findings indicate two parallel tracks to capitalize on our work: 1) Further development of advanced materials to modulate the response to mechanical and molecular factors and 2) Research into mechanisms and neuroprotective pathways, specifically M2 macrophage/microglia presence, CSPG reduction, and vimentin upregulation.

Acknowledgments

This work was supported by Grant Number R21-NS053798 and F31-NS063640 from the National Institute of Neurological Disorders and Stroke and T32-EB004314-06 for the National Institute of Biomedical Imaging and Bioengineering. Additional support was from Veteran's Affairs grants C3819C, F4827H and B6344W. The authors acknowledge the support of Anne DeChant and Dr. Horst von Recum. None of the funding sources aided in the collection, analysis, and interpretation of data, in the writing of the report, or in the decision to submit the paper for publication.

References

Alberts, B. Molecular Biology of the Cell. Alberts, B., et al., editors. Garland Publishing Inc.; New York, New York: 1994. p. 948-1009.

Alonso G. NG2 proteoglycan-expressing cells of the adult rat brain: possible involvement in the formation of glial scar astrocytes following stab wound. Glia. 2005; 49:318–38. [PubMed: 15494983]

Biran R, Martin DC, Tresco PA. Neuronal cell loss accompanies the brain tissue response to chronically implanted silicon microelectrode arrays. Exp Neurol. 2005; 195:115–26. [PubMed: 16045910]

Biran R, Martin DC, Tresco PA. The brain tissue response to implanted silicon microelectrode arrays is increased when the device is tethered to the skull. J Biomed Mater Res A. 2007; 82:169–78. [PubMed: 17266019]

Busch SA, Horn KP, Cuascut FX, Hawthorne AL, Bai L, Miller RH, Silver J. Adult NG2+ cells are permissive to neurite outgrowth and stabilize sensory axons during macrophage-induced axonal dieback after spinal cord injury. J Neurosci. 2010; 30:255–65. [PubMed: 20053907]

Busch SA, Silver J. The role of extracellular matrix in CNS regeneration. Current opinion in neurobiology. 2007; 17:120–7. [PubMed: 17223033]

Buzsáki G. Large-scale recording of neuronal ensembles. Nat Neurosci. 2004; 7:446–51. [PubMed: 15114356]

Capadona JR, Shanmuganathan K, Trittschuh S, Seidel S, Rowan SJ, Weder C. Polymer nanocomposites with nanowhiskers isolated from microcrystalline cellulose. Biomacromolecules. 2009; 10:712–6. [PubMed: 19256493]

Capadona JR, Shanmuganathan K, Tyler DJ, Rowan SJ, Weder C. Stimuli-Responsive Polymer Nanocomposites Inspired by the Sea Cucumber Dermis. Science. 2008; 319:1370. [PubMed: 18323449]

Capadona JR, Van Den Berg O, Capadona LA, Schroeter M, Rowan SJ, Tyler DJ, Weder C. A versatile approach for the processing of polymer nanocomposites with self-assembled nanofibre templates. Nat Nano. 2007; 2:765–9.

Clark K, Langeslag M, Figdor CG, van Leeuwen FN. Myosin II and mechanotransduction: a balancing act. Trends in cell biology. 2007; 17:178–86. [PubMed: 17320396]

Cullen DK, Simon CM, LaPlaca MC. Strain rate-dependent induction of reactive astrogliosis and cell death in three-dimensional neuronal-astrocytic co-cultures. Brain Res. 2007; 1158:103–15. [PubMed: 17555726]

Engler AJ, Sen S, Sweeney HL, Discher DE. Matrix elasticity directs stem cell lineage specification. Cell. 2006; 126:677–89. [PubMed: 16923388]

Faulkner JR, Herrmann JE, Woo MJ, Tansey KE, Doan NB, Sofroniew MV. Reactive astrocytes protect tissue and preserve function after spinal cord injury. J Neurosci. 2004; 24:2143–55. [PubMed: 14999065]

Fawcett JW, Asher RA. The glial scar and central nervous system repair. Brain research bulletin. 1999; 49:377–91. [PubMed: 10483914]

Flanagan LA, Ju YE, Marg B, Osterfield M, Janmey PA. Neurite branching on deformable substrates. Neuroreport. 2002; 13:2411–5. [PubMed: 12499839]

Frampton JP, Hynd MR, Shuler ML, Shain W. Effects of Glial Cells on Electrode Impedance Recorded from Neural Prosthetic Devices In Vitro. Annals of biomedical engineering. 2010

Fujita T, Yoshimine T, Maruno M, Hayakawa T. Cellular dynamics of macrophages and microglial cells in reaction to stab wounds in rat cerebral cortex. Acta neurochirurgica. 1998; 140:275–9. [PubMed: 9638265]

Georges PC, Miller WJ, Meaney DF, Sawyer ES, Janmey PA. Matrices with compliance comparable to that of brain tissue select neuronal over glial growth in mixed cortical cultures. Biophysical journal. 2006; 90:3012–8. [PubMed: 16461391]

Harris J, Hess AE, Rowan S, Weder C, Zorman C, Tyler D, Capadona J. In vivo deployment of mechanically adaptive nanocomposites for intracortical microelectrodes. Journal of Neural Engineering. 2011; 8:046010. [PubMed: 21654037]

Horn KP, Busch SA, Hawthorne AL, van Rooijen N, Silver J. Another Barrier to Regeneration in the CNS: Activated Macrophages Induce Extensive Retraction of Dystrophic Axons through Direct Physical Interactions. 2008

Ingber DE. Cellular mechanotransduction: putting all the pieces together again. Faseb J. 2006; 20:811–27. [PubMed: 16675838]

Kigerl KA, Gensel JC, Ankeny DP, Alexander JK, Donnelly DJ, Popovich PG. Identification of two distinct macrophage subsets with divergent effects causing either neurotoxicity or regeneration in the injured mouse spinal cord. J Neurosci. 2009; 29:13435–44. [PubMed: 19864556]

Kim YT, Hitchcock RW, Bridge MJ, Tresco PA. Chronic response of adult rat brain tissue to implants anchored to the skull. Biomaterials. 2004; 25:2229–37. [PubMed: 14741588]

Kippert A, Fitzner D, Helenius J, Simons M. Actomyosin contractility controls cell surface area of oligodendrocytes. BMC cell biology. 2009; 10:71. [PubMed: 19781079]

Kreutzberg GW. Microglia: a sensor for pathological events in the CNS. Trends in neurosciences. 1996; 19:312–8. [PubMed: 8843599]

Lee H, Bellamkonda RV, Sun W, Levenston ME. Biomechanical analysis of silicon microelectrode-induced strain in the brain. J Neural Eng. 2005; 2:81–9. [PubMed: 16317231]

Lee K, He J, Clement R, Massia S, Kim B. Biocompatible benzocyclobutene (BCB)-based neural implants with micro-fluidic channel. Biosens Bioelectron. 2004; 20:404–7. [PubMed: 15308247]

Levin EC, Acharya NK, Sedeyn JC, Venkataraman V, D'Andrea MR, Wang HY, Nagele RG. Neuronal expression of vimentin in the Alzheimer's disease brain may be part of a generalized dendritic damage-response mechanism. Brain Res. 2009; 1298:194–207. [PubMed: 19728994]

Liu X, McCreery DB, Carter RR, Bullara LA, Yuen TG, Agnew WF. Stability of the interface between neural tissue and chronically implanted intracortical microelectrodes. IEEE Trans Rehabil Eng. 1999; 7:315–26. [PubMed: 10498377]

Lu Y, Wang D, Li T, Zhao X, Cao Y, Yang H, Duan YY. Poly(vinyl alcohol)/poly(acrylic acid) hydrogel coatings for improving electrode-neural tissue interface. Biomaterials. 2009; 30:4143–51. [PubMed: 19467702]

McConnell GC, Rees HD, Levey AI, Gutekunst CA, Gross RE, Bellamkonda RV. Implanted neural electrodes cause chronic, local inflammation that is correlated with local neurodegeneration. J Neural Eng. 2009; 6:56003.

McConnell GC, Schneider TM, Owens DJ, Bellamkonda RV. Extraction force and cortical tissue reaction of silicon microelectrode arrays implanted in the rat brain. IEEE Trans Biomed Eng. 2007; 54:1097–107. [PubMed: 17554828]

McKeon RJ, Jurynec MJ, Buck CR. The chondroitin sulfate proteoglycans neurocan and phosphacan are expressed by reactive astrocytes in the chronic CNS glial scar. J Neurosci. 1999; 19:10778–88. [PubMed: 10594061]

Nikles, SA.; Pellinen, DS.; Kitagawa, J.; Bradley, RM.; Kipke, DR.; Najafi, K. Long term in vitro monitoring of polyimide microprobe electrical properties. Engineering in Medicine and Biology Society, 2003. Proceedings of the 25th Annual International Conference of the IEEE; 2003.

Nisbet DR, Rodda AE, Horne MK, Forsythe JS, Finkelstein DI. Neurite infiltration and cellular response to electrospun polycaprolactone scaffolds implanted into the brain. Biomaterials. 2009

Nishiyama A. Polydendrocytes: NG2 cells with many roles in development and repair of the CNS. Neuroscientist. 2007; 13:62–76. [PubMed: 17229976]

Ortinski PI, Dong J, Mungenast A, Yue C, Takano H, Watson DJ, Haydon PG, Coulter DA. Selective induction of astrocytic gliosis generates deficits in neuronal inhibition. Nat Neurosci. 2010; 13:584–91. [PubMed: 20418874]

Ostrow LW, Sachs F. Mechanosensation and endothelin in astrocytes--hypothetical roles in CNS pathophysiology. Brain Res Brain Res Rev. 2005; 48:488–508. [PubMed: 15914254]

Pekny, M. Glial Cell Function. Lopez, BC.; Nieto-Sampedro, M., editors. Elsevier; Amsterdam: 2003.

Pinheiro, J.; Bates, D.; DebRoy, S.; Sarkar, D.; the R Core team. nlme: Linear and Nonlinear Mixed Effects Models. 2009.

R Development Core Team. R: A language and environment for statistical computing. R Foundation for Statistical Computing; Vienna, Austria: 2009.

Roitbak T, Sykova E. Diffusion barriers evoked in the rat cortex by reactive astrogliosis. Glia. 1999; 28:40–8. [PubMed: 10498821]

Shanmuganathan K, Capadona JR, Rowan SJ, Weder C. Stimuli-Responsive Mechanically Adaptive Polymer Nanocomposites. ACS Applied Materials & Interfaces. 2009; 2:165–74. [PubMed: 20305827]

Shanmuganathan K, Capadona JR, Rowan SJ, Weder C. Bio-inspired mechanically-adaptive nanocomposites derived from cotton cellulose whiskers. Journal of Materials Chemistry. 2010a; 20:180.

Shanmuganathan K, Capadona JR, Rowan SJ, Weder C. Biomimetic mechanically adaptive nanocomposites. Progress in Polymer Science. 2010b; 35:212–22.

Shearer MC, Niclou SP, Brown D, Asher RA, Holtmaat AJ, Levine JM, Verhaagen J, Fawcett JW. The astrocyte/meningeal cell interface is a barrier to neurite outgrowth which can be overcome by manipulation of inhibitory molecules or axonal signalling pathways. Molecular and cellular neurosciences. 2003; 24:913–25. [PubMed: 14697658]

Silver J, Miller JH. Regeneration beyond the glial scar. Nature reviews. 2004; 5:146–56.

Simard M, Arcuino G, Takano T, Liu QS, Nedergaard M. Signaling at the gliovascular interface. J Neurosci. 2003; 23:9254–62. [PubMed: 14534260]

Subbaroyan, J. Biomedical Engineering. University of Michigan; Ann Arbor, MI: 2007. Investigations of tethering induced injury response in brain tissue by intracortical implants through modeling and in vivo experiments.

Subbaroyan J, Martin DC, Kipke DR. A finite-element model of the mechanical effects of implantable microelectrodes in the cerebral cortex. J Neural Eng. 2005; 2:103–13. [PubMed: 16317234]

Szarowski DH, Andersen MD, Retterer S, Spence AJ, Isaacson M, Craighead HG, Turner JN, Shain W. Brain responses to micro-machined silicon devices. Brain Res. 2003; 983:23–35. [PubMed: 12914963]

Takeuchi S, Suzuki T, Mabuchi K, Fujita H. 3D flexible multichannel neural probe array. Journal of Micromechanics and Microengineering. 2004; 14:104–7.

Takeuchi S, Ziegler D, Yoshida Y, Mabuchi K, Suzuki T. Parylene flexible neural probes integrated with microfluidic channels. Lab Chip. 2005; 5:519–23. [PubMed: 15856088]

Watson RE Jr, Wiegand SJ, Clough RW, Hoffman GE. Use of cryoprotectant to maintain long-term peptide immunoreactivity and tissue morphology. Peptides. 1986; 7:155–9. [PubMed: 3520509]

Wester BA, Lee RH, LaPlaca MC. Development and characterization of in vivo flexible electrodes compatible with large tissue displacements. J Neural Eng. 2009; 6:024002. [PubMed: 19255461]

Winslow BD, Christensen MB, Yang WK, Solzbacher F, Tresco PA. A comparison of the tissue response to chronically implanted Parylene-C-coated and uncoated planar silicon microelectrode arrays in rat cortex. Biomaterials. 2010

Winslow BD, Tresco PA. Quantitative analysis of the tissue response to chronically implanted microwire electrodes in rat cortex. Biomaterials. 2009

Zhong Y, Bellamkonda RV. Dexamethasone-coated neural probes elicit attenuated inflammatory response and neuronal loss compared to uncoated neural probes. Brain Res. 2007; 1148:15–27. [PubMed: 17376408]

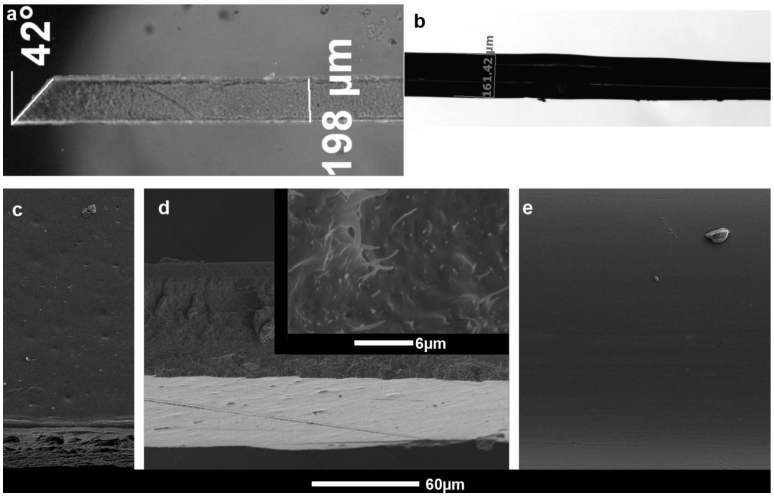

Figure 1.

Materials bilaterally implanted in rodent cortex. a) Microscopic picture of PVAc-NC polymer nanocomposite implant, 3mm in length, 200µm wide, 100µm thick. b) Microscopic picture of PVAc-coated tungsten wire. The tungsten wire is 50µm in diameter before coating. The diameter after coating is ~160µm. Light white lines outline the wire within the PVAc coating. c–e) SEM images of implants. c) SEM image of pressed side of PVAc-NC implant. d) SEM image showing cut side of PVAc-NC implant that is rough. The image also shows the pressed side of the PVAc-NC implant at the bottom of the image. Inset, a higher magnification SEM image shows the cellulose whiskers on the cut side of the PVAc-NC implant. e) SEM image of the PVAc-coated tungsten wire.

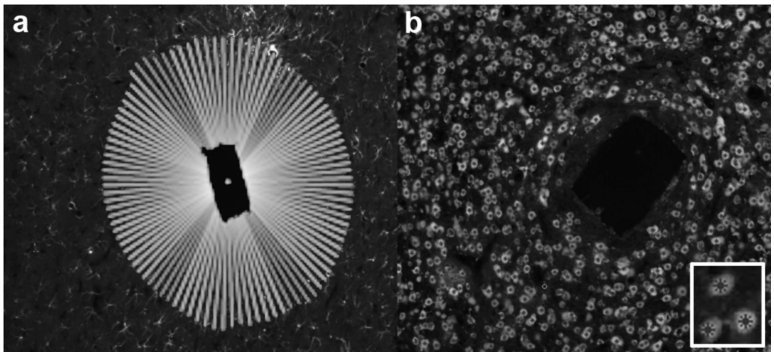

Figure 2.
Quantification of fluorescent immunohistochemistry (fIHC) staining via two methods. Horizontal slices of representative brains shown. a) Representative image indicating the 100 radial lines drawn to compute the pixel intensity radiating outward from electrode – tissue interface. b) Representative image showing computer and user selected cell bodies to compute the distance of cell bodies from the electrode – tissue interface. Inset, Close-up of marked cell bodies.

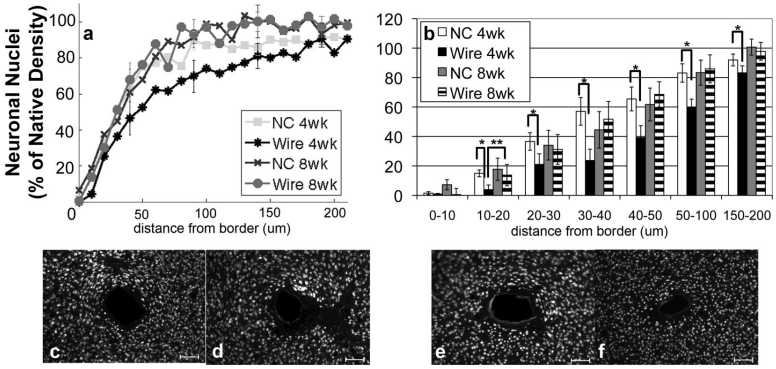

Figure 3.

Analysis of NeuN Immunohistochemistry. a) Quantification of NeuN based on distance from the tissue-implant border in response to implants: four week NC (square), four week wire (asterisk), eight week NC (cross), eight week wire (circle). Points represent histogram counts in 10 μm intervals. Counts have been scaled based on area as well as background count per image. b) Average count of NeuN as a function of distance from the tissue-implant border ± standard error. Four week NC (white), four week wire (black), eight week NC (gray), eight week wire (striped) *= $p<0.05$ for intraweek comparisons, **<0.05 for interweek comparisons.

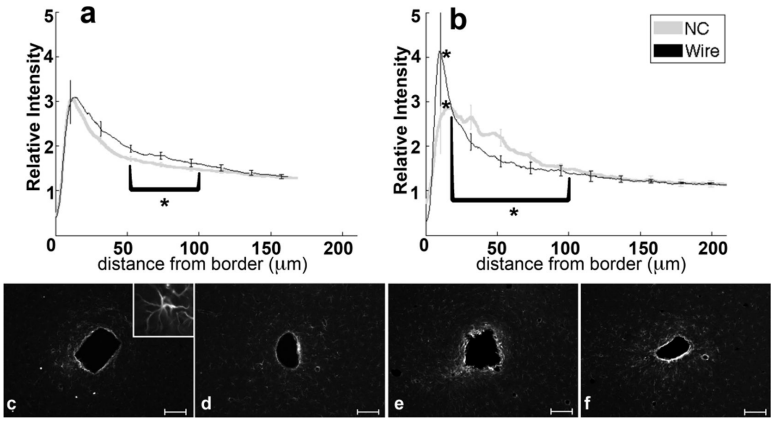

Figure 4.

Analysis of GFAP-Reactive Astrocytes as a function of distance from the tissue-implant border. a) Relative intensity ± standard error as a function of distance from border of four week NC (gray) and wire (black). Brackets indicate an integral of intensity. b) Relative intensity ± standard error as a function of distance from border of eight week NC (gray) and wire (black). Representative images of GFAP for c) four week NC, inset 50μm wide close-up of reactive astrocyte, d) four week wire, e) eight week NC, and f) eight week wire. Scale bars 100 μm. *=$p<0.05$.

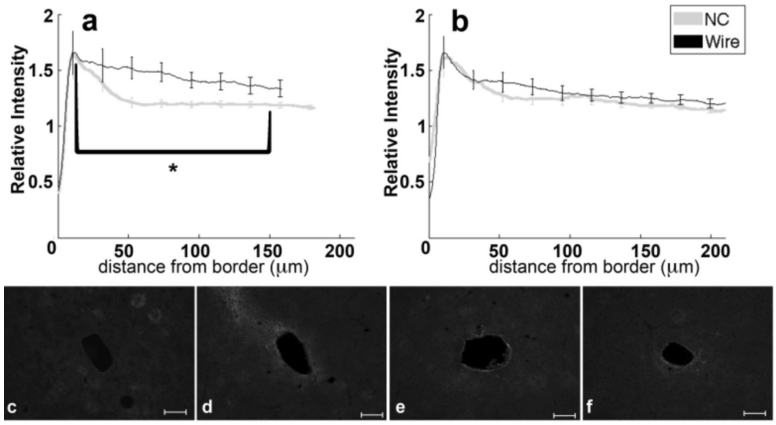

Figure 5.

Analysis of CS56-CSPGs as a function of distance. a) Relative intensity ± standard error as a function of distance from border of four week NC (gray) and wire (black). Brackets indicate an interval of integral of intensity calculation. b) Relative intensity ± standard error as a function of distance from border of eight week NC (gray) and wire (black). Representative images of CS56 for c) four week NC, d) four week wire, e) eight week NC, and f) eight week wire. Scale bars 100 μm.*=$p<0.05$.

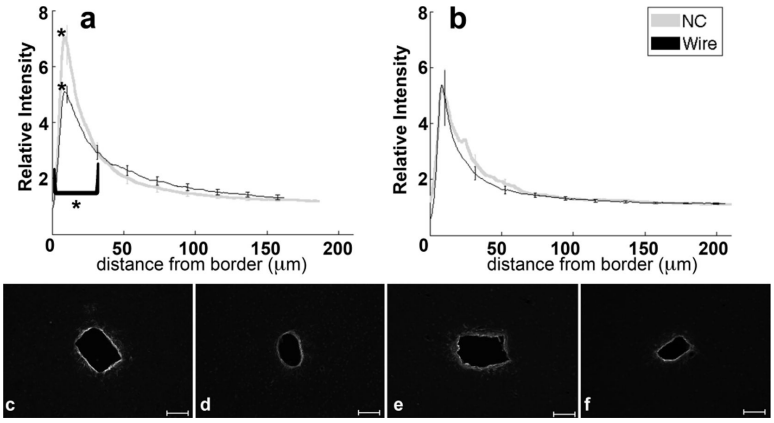

Figure 6.

Analysis of vimentin as a function of distance. a) Relative intensity ± standard error as a function of distance from border of four week NC (gray) and wire (black). Brackets indicate an integral of intensity. b) Relative intensity ± standard error as a function of distance from border of eight week NC (gray) and wire (black). Representative images of vimentin for c) four week NC, d) four week wire, e) eight week NC, and f) eight week wire. Scale bars 100 μm.*= $p<0.05$.

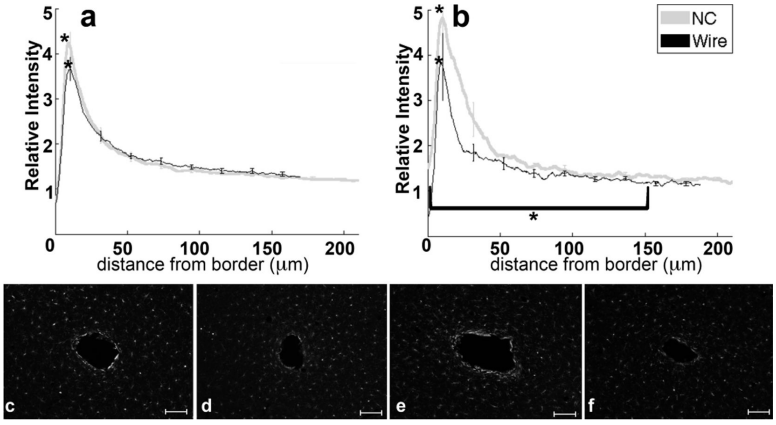

Figure 7.

Analysis of IBA1-Microglia immunohistochemistry as a function of distance from the tissue-implant border. a) Relative intensity ± standard error as a function of distance from border of four week NC (gray) and wire (black). Brackets indicate an integral of intensity. b) Relative intensity ± standard error as a function of distance from border of eight week NC (gray) and wire (black). Representative images of IBA1 for c) four week NC, d) four week wire, e) eight week NC, and f) eight week wire. Scale bars 100 μm. *= $p<0.05$.

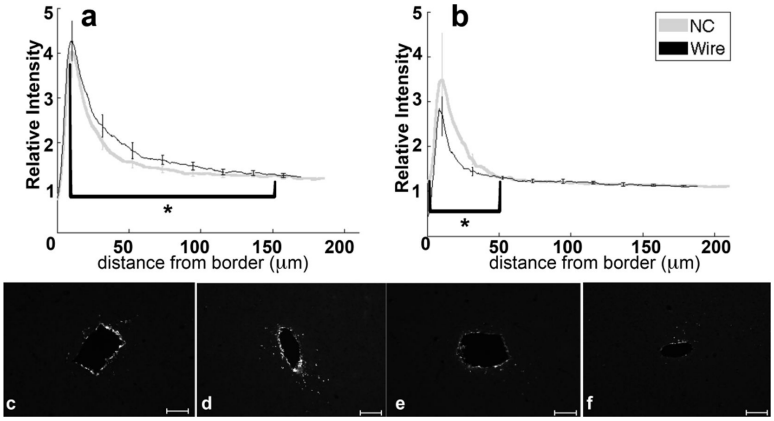

Figure 8.

Analysis of ED1-Activated Macrophage and Microglia immunohistochemistry as a function of distance from the tissue-implant border. a) Relative intensity ± standard error as a function of distance from border of four week NC (gray) and wire (black). Brackets indicate an integral of intensity. b) Relative intensity ± standard error as a function of distance from border of eight week NC (gray) and wire (black). Representative images of vimentin for c) four week NC, d) four week wire, e) eight week NC, and f) eight week wire. Scale bars 100 μm. *= $p<0.05$.

Table 1

Summary of Primary Antibodies.

Antibody	Vendor (Part #)	Dilution	Isotype	Cell Type/Labeling
GFAP	Chemicon (AB5804)	1:1000	Rb IgG	Astrocytes
NeuN	Chemicon (MAB377)	1:500	Ms IgG1	Neurons
CD68 (EDI)	Chemicon (MAB1435)	1:250	Ms IgG1	Activated Macrophages, Microglia
IBA1	Wako (019–19741)	1:615	Rb IgG	Microglia
CS56	Sigma (C8035)	1:500	Ms IgM	Chondroitin Sulfate Proteoglycans
Vimentin	Sigma (V6389)	1:200	Ms IgG1	Varied- Immature/reactive astrocytes, microglia, endothelial cells, and fibroblasts

Table 2

Summary of IHC analysis when subdivided based on side. The number in the table represents the number of sections analyzed that showed a measurable difference in normalized stain intensity for one side or the other. The results are further divided into measures within the first 50 μm and the first 20 μm. These correspond to the distance related to unit recordings and approximately the first 3–4 cell layers, respectively. There does not appear to be any particular bias in the results to one side or the other and that surface roughness is not significantly contributing to the response.

Label	DAPI			EDI		
Greater side	Long side	Short side	No Difference	Long Side	Short side	No Difference
Within 50 μm	13	12	13	6	13	12
Within 20 μm	10	9	19	7	12	12